Planta (2014) 240:585–598
DOI 10.1007/s00425-014-2108-0

ORIGINAL ARTICLE

Subcellular distribution of central carbohydrate metabolism pathways in the red alga *Cyanidioschyzon merolae*

Takashi Moriyama · Kenta Sakurai · Kohsuke Sekine · Naoki Sato

Received: 31 March 2014 / Accepted: 10 June 2014 / Published online: 10 July 2014

Abstract

Main conclusion **Comprehensive subcellular localization analysis revealed that the subcellular distribution of carbohydrate metabolic pathways in the red alga *Cyanidioschyzon* is essentially identical with that in *Arabidopsis*, except the lack of transaldolase.**

In plants, the glycolysis and oxidative pentose phosphate pathways (oxPPP) are located in both cytosol and plastids. However, in algae, particularly red algae, the subcellular localization of enzymes involved in carbon metabolism is unclear. Here, we identified and examined the localization of enzymes related to glycolysis, oxPPP, and tricarboxylic acid (TCA) and Calvin–Benson cycles in the red alga *Cyanidioschyzon merolae*. A gene encoding transaldolase of the oxPPP was not found in the *C. merolae* genome, and no transaldolase activity was detected in cellular extracts. The subcellular localization of 65 carbon metabolic enzymes tagged with green fluorescent protein or hemagglutinin was examined in *C. merolae* cells. As expected, TCA and Calvin–Benson cycle enzymes were localized to mitochondria and plastids, respectively. The analyses also revealed that the cytosol contains the entire glycolytic pathway and partial oxPPP, whereas the plastid contains a partial glycolytic pathway and complete oxPPP, with the exception of transaldolase. Together, these results suggest that the subcellular distribution of carbohydrate metabolic pathways in *C. merolae* is essentially identical with that reported in the photosynthetic tissue of *Arabidopsis thaliana*; however, it appears that substrates typically utilized by transaldolase are consumed by glycolytic enzymes in the plastidic oxPPP of *C. merolae*.

Keywords Glycolysis · Oxidative pentose phosphate pathway · Tricarboxylic acid cycle · Calvin–Benson cycle · Subcellular localization · Red algae

Introduction

Nearly all organisms possess functional glucose metabolic pathways, such as the glycolytic and oxidative pentose phosphate pathways (oxPPP), which are localized in the cytosol in non-photosynthetic eukaryotes. Glycolysis converts glucose into pyruvate, producing two moles of ATP and two moles of NADH per one mole of glucose, whereas the oxPPP produces NADPH and pentoses, rather than ATP. The produced pyruvate is converted into citrate, which is further oxidized in the mitochondria by the tricarboxylic acid (TCA) cycle through a series of eight enzyme-catalyzed reactions. In photosynthetic organisms, an additional carbohydrate metabolic pathway known as the Calvin–Benson cycle, which is also referred to as the reductive pentose phosphate pathway, produces the triosephosphate glyceraldehyde-3-phosphate (GAP).

Electronic supplementary material The online version of this article (doi:10.1007/s00425-014-2108-0) contains supplementary material, which is available to authorized users.

T. Moriyama (✉) · K. Sakurai · N. Sato
Department of Life Sciences, Graduate School of Arts and Sciences, The University of Tokyo, Komaba 3-8-1, Meguro-ku, Tokyo 153-8902, Japan
e-mail: moripoly@bio.c.u-tokyo.ac.jp

T. Moriyama · K. Sakurai · K. Sekine · N. Sato
JST, CREST, K's Gobancho, 7 Gobancho, Chiyoda-ku, Tokyo 102-0076, Japan

K. Sekine
Division of Life Sciences, Komaba Organization for Educational Excellence, College of Arts and Sciences, The University of Tokyo, Komaba 3-8-1, Meguro-ku, Tokyo 153-8902, Japan

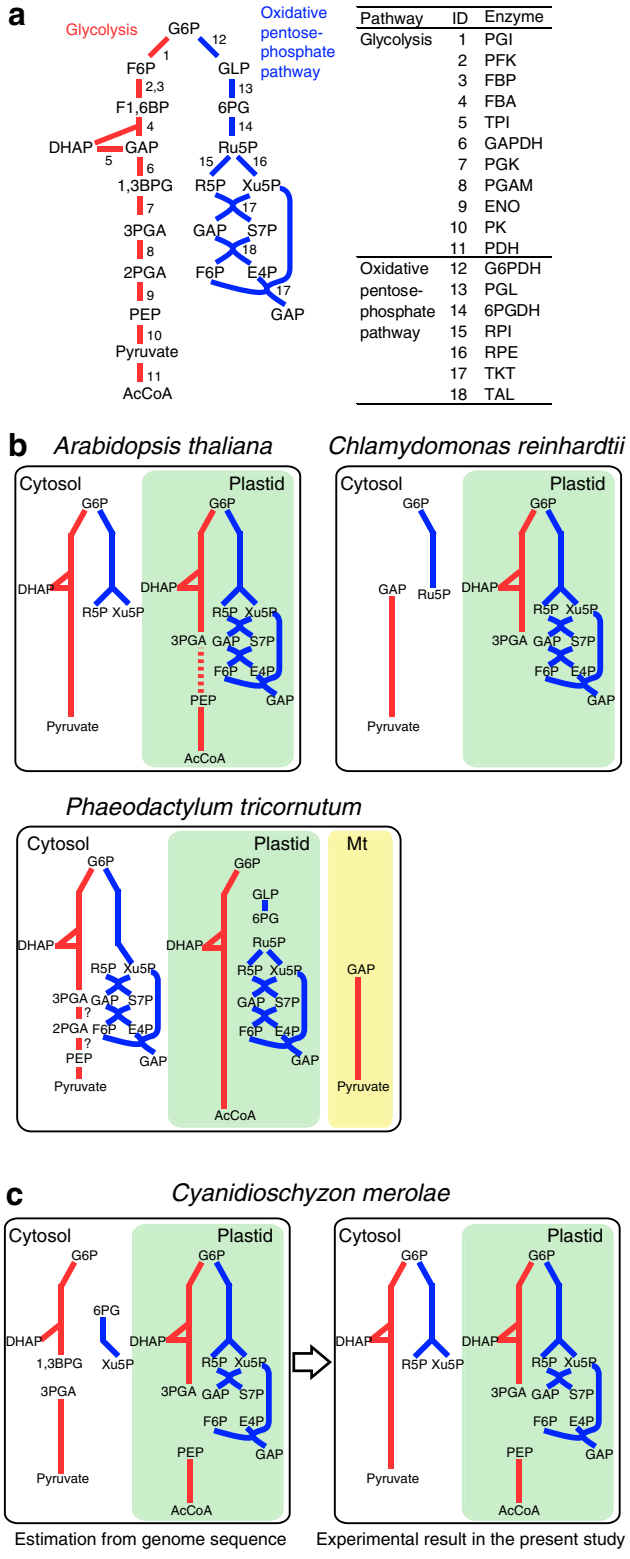

Pathway	ID	Enzyme
Glycolysis	1	PGI
	2	PFK
	3	FBP
	4	FBA
	5	TPI
	6	GAPDH
	7	PGK
	8	PGAM
	9	ENO
	10	PK
	11	PDH
Oxidative pentose-phosphate pathway	12	G6PDH
	13	PGL
	14	6PGDH
	15	RPI
	16	RPE
	17	TKT
	18	TAL

Fig. 1 Subcellular distribution of glycolytic and oxidative pentose phosphate pathways (oxPPP) in plants and algae. **a** General glycolytic pathway (*red line*) and oxPPP (*blue line*). Numbers between intermediates indicate the reaction process ID, and the corresponding enzymes are shown in the table to the *right*. Abbreviations of intermediates are shown in Fig. 3. Unabridged enzyme names are shown in Table 1 and Online Resource Table S 1. **b** Glycolysis and oxPPP reported in the plant *Arabidopsis thaliana*, green alga *Chlamydomonas reinhardtii*, and diatom *Phaeodactylum tricornutum*. Metabolic map of *A. thaliana* was made from the data listed in Online Resource Table S 1. PGAM and ENO have not been reported in greening chloroplasts in *A. thaliana*, and the *dotted line* indicates a reaction step that occurs only in non-photosynthetic tissue. The pathway map of *C. reinhardtii* and *P. tricornutum* were drawn from data in the studies by Johnson and Alric (2013) and Gruber et al. (2009), respectively. **c** Glycolysis and oxPPP estimated from the genome sequence of *C. merolae* (*left*) and the pathways verified by experimental results in the present study (*right*). The transaldolase gene was not found in the *C. merolae* genome, and no transaldolase activity was detected in cell extracts (Online Resource Fig. S 2)

In flowering plants, glycolysis and oxPPP exist in two compartments: the cytosol and plastids (Dennis and Miernyk 1982). A total of 105 enzymes related to glycolysis and oxPPP have been identified in *Arabidopsis thaliana* (Online Resource Table S 1), and their subcellular localization has been examined by various approaches, including green fluorescent protein (GFP) fusion protein analysis, enzymatic activity measurements in isolated organelles, and proteome analysis. In photosynthetic tissues of *Arabidopsis*, nearly all glycolytic enzymes, from phosphoglucose isomerase (PGI) to pyruvate kinase (PK) in the reaction process (process ID [ID]: 1–10; Fig. 1a), are present in the cytosol, although several enzymes, from PGI to phosphoglycerate kinase (PGK) (ID: 1–7), and PK to pyruvate dehydrogenase (PDH) (ID: 10 and 11) are also found in plastids (Fig. 1b). Recently, the plastid localization of phosphoglycerate mutase (PGAM, ID: 8) and enolase (ENO, ID: 9) has also been reported in non-photosynthetic tissues (Andriotis et al. 2010). All cytosolic enzymes related to glycolysis in *Arabidopsis* are associated with the mitochondrial outer membrane (Giegé et al. 2003), a configuration that is considered to allow the direct supply of pyruvate to the mitochondria as a substrate of the TCA cycle. In *A. thaliana*, plastids contain a complete set of oxPPP enzymes (ID: 12–18), whereas the cytosol only contains five oxPPP-related enzymes (ID: 12–16), and lacks the transketolase (TKT, ID: 17) and transaldolase (TAL, ID: 18) (Fig. 1b). Despite extensive studies, localization analysis of these two pathways in *A. thaliana* remains incomplete, as the *Arabidopsis* genome encodes a large number of redundant genes.

In the green alga *Chlamydomonas reinhardtii*, subcellular compartmentalization of enzymes related to carbohydrate metabolic pathways has been mainly examined by enzymatic activity and proteome analyses of isolated organelles (reviewed in Johnson and Alric 2013). These studies have demonstrated that the cytosol contains enzymes involved in the latter half of glycolysis (ID: 6–10) and the first half of oxPPP (ID: 12–14), whereas the plastid

includes enzymes for the first half of glycolysis (ID: 1–7) and a complete complement of oxPPP enzymes (ID: 12–18) (Fig. 1b). Although localization data of metabolic enzymes are relatively limited in other algae, it was reported that glycolytic enzymes in diatoms are localized to the mitochondria (ID: 6–10) in addition to the cytosol (ID: 1–10) and plastids (ID: 1–11) (Liaud et al. 2000). Thus, it appears that differences in the compartmentation of enzymes lead to diversification of glycolysis and oxPPP pathways in photosynthetic eukaryotes. However, comprehensive localization analysis in individual organisms is necessary to understand cellular carbohydrate metabolism.

Cyanidioschyzon merolae is a unicellular rhodophyte that inhabits hot springs with warm water (up to 50 °C) that is acidified by sulfuric acid (pH 1.5–2.5). *C. merolae* has a simple cell structure consisting of a single mitochondrion and plastid per cell, and is therefore a suitable model for subcellular localization analyses. In addition, the nuclear (Matsuzaki et al. 2004; Nozaki et al. 2007), plastid (Ohta et al. 2003) and mitochondrial genomes (Ohta et al. 1998) of this alga are completely sequenced. The *C. merolae* genome is small (16.5 Mbp) and contains a small number of predicted protein-coding genes (4,775 genes) with low redundancy. *C. merolae* is also readily transformed with polyethylene glycol (PEG) (Ohnuma et al. 2008) and has been successfully used for subcellular localization experiments with transformants expressing 3× hemagglutinin (HA)-tagged and GFP-fused proteins (Ohnuma et al. 2008; Moriyama et al. 2014; Watanabe et al. 2011). Genomic analyses for genes related to carbon metabolism suggest that *C. merolae* encodes metabolic pathways for floridoside, trehalose, storage glucans, and matrix polysaccharides (Barbier et al. 2005). *C. merolae* is also predicted to possess a minimal set of metabolic transporters, such as those for triose phosphate, but no plastidic dicarboxylate translocators, which are required for nitrogen assimilation and photorespiration pathway and are conserved in green plants and algae (Barbier et al. 2005; Tyra et al. 2007). Our laboratory has identified a unique pathway for lipid biosynthesis in *C. merolae* based on the results of genomic and experimental analyses (Sato and Moriyama 2007). However, identification and subcellular localization of enzymes related to central carbohydrate metabolic pathways remain unclear.

In the present study, we searched for the enzymes in *C. merolae* related to glycolysis, oxPPP, and the TCA and Calvin–Benson cycles, and analyzed their subcellular localization by the observation of GFP- and 3× hemagglutinin (HA)-fusion proteins. This comprehensive approach revealed several similarities and differences in the type and localization of enzymes involved in carbohydrate metabolic pathways of photosynthetic eukaryotes.

Materials and methods

Culture conditions and transformation of *C. merolae*

Cells of *C. merolae* strain 10D (Toda et al. 1998) were inoculated into 100 mL 2× Allen's medium (pH 2.5; Minoda et al. 2004) in 200-mL flasks. Flasks were shaken under continuous light provided by three fluorescent tubes (30 μmol m^{-2} s^{-1}) at 40 °C. Cultured *C. merolae* cells were transformed by the PEG-method, as described by Moriyama et al. (2014), and transformed cells were cultured overnight at 40 °C with aeration by 1 % CO_2.

Overexpression and purification of *Anabaena* Xfp protein

The full-length sequence of the *xfp* gene (*all2567*) was amplified by PCR from the *Anabaena* sp. PCC 7120 genome (laboratory stock) using the primer pair InF_pThioA_AnaXfp-F (5′-CCTCTAGAGTCGACCTGCAGTACTTTAGCAAGTCCTCCACA-3′) and InF_pThioA_AnaXfp-R (5′-ACCCTGTACGATTACTGCAGCTAATACGGCCATTGCCAGT-3′). The underlined sequences correspond to the ends of *Pst*I-linearized pThioHisA vector (Invitrogen, Carlsbad, CA, USA) and are required for the In-Fusion cloning reaction (Clontech Laboratories, Mountain View, CA, USA). The PCR product was cloned into *Pst*I-digested pThioHisA using the In-Fusion reaction, as directed by the manufacturer (Clontech Laboratories). Overexpression in *Escherichia coli* TOP10 and purification of recombinant protein were performed as described previously (Moriyama et al. 2008).

Preparation of protein extract

For measurement of transaldolase activity, soluble protein was extracted from *C. merolae* cells. *C. merolae* cells were grown to mid-log phase ($OD_{750} = 0.8$) and collected by centrifugation at 1,500*g* for 10 min. The cell pellet was resuspended in protein extraction buffer (100 mM Tris–HCl pH 8.0, 50 mM KCl, 5 mM $MgCl_2$, 1 mM EDTA, and 3 mM dithiothreitol) and was then disrupted by sonication. The supernatant was obtained by centrifugation of the lysed cell suspension at 18,000*g* for 15 min.

Transaldolase assay

Because erythrose 4-phosphate (E4P) was not commercially available, it was produced enzymatically from fructose 6-phosphate (F6P) by the phosphoketolase reaction with purified Xfp (Meile et al. 2001). The phosphoketolase reaction was performed in 4 mL Xfp reaction mixture (33.3 mM KH_2PO_4 [pH 6.5], 25 mM F6P, 1 mM thiamine

pyrophosphate, and 150 μg Xfp recombinant protein) at 30 °C for 3 h. In this reaction, equimolar amounts of acetyl-phosphate and E4P were produced. The concentration of acetyl-phosphate was measured spectrophotometrically as ferric acetyl hydroxamate by the procedure of Racker (1962).

Transaldolase activity was measured photometrically by following the A_{340} change of NADH according to a modified procedure of Soderberg and Alver (2004). Briefly, 2 mL transaldolase reaction mixture [50 mM HEPES–KOH (pH 7.6), 5 mM $MgCl_2$, 1 mM EDTA, 46 units of triosephosphate isomerase (TPI; Sigma-Aldrich, St. Louis, MO, USA), 2 units glycerol 3-phosphate dehydrogenase (Sigma-Aldrich), 200 μM NADH, *C. merolae* protein extract, and 100 μL Xfp-reaction mixture] containing a final concentration of 150 μM E4P and 1 mM F6P was reacted at 30 °C and monitored at A_{340} for 1 min. As a positive control, yeast transaldolase (Sigma-Aldrich) was added to the mixture instead of *C. merolae* protein extract. In this assay, transaldolase activity produces glyceraldehyde 3-phosphate (GAP) and sedoheptulose 7-phosphate (S7P) from F6P and E4P, and the produced GAP is then converted to dihydroxyacetone phosphate (DHAP) by TPI. DHAP is then reduced to glycerol phosphate by glycerol 3-phosphate dehydrogenase with concomitant oxidation of NADH to NAD^+. The decrease in A_{340} was monitored during the reaction as a measure of transaldolase activity.

Construction of GFP- and 3× hemagglutinin (3× HA)-fusion genes

Carbohydrate metabolism-related genes and their promoter sequences were amplified by PCR with specific primer sets (Online Resource Table S 2). For the construction of GFP-fusion genes, the cauliflower mosaic virus 35S promoter was first excised from the sGFP (S65T) vector (Chiu et al. 1996) by digestion with *Xba*I. PCR-amplified DNA fragments were then inserted into the promotorless sGFP (S65T) vector using the appropriate restriction enzymes or the In-Fusion HD cloning kit (Clontech Laboratories).

For overexpression of GFP fusion genes, the amplified DNA fragments were inserted into pCG1 vector, which contains the *apcC* promoter of *C. merolae*, sGFP, and NOS terminator (Watanabe et al. 2011). For the construction of 3× HA-fusion genes, the target DNA fragments were inserted into pBSHAb-T3′ vector using the appropriate restriction enzymes or the In-Fusion cloning kit (Ohnuma et al. 2008).

For the construction of *N*-terminal fusion of 3× HA-tag with citrate synthases expressed by the *apcC* promoter, first, the *apcC* promoter, which was amplified by PCR with *C. merolae* genome as a template with primers (5′-ATGCCCGCGGTTACAATACCGATAGATGAGTTTCG -3′ and 5′-GCATCTGCAGGGATCCTCTAGAGGTCAACGAACGA-3′; underlined sequences are restriction sites of *Pac*II and *Pst*I, respectively), was inserted into pBSHAb-T3′ vector using *Pac*II and *Pst*I. The DNA fragments of citrate synthases were inserted into pBSHAb-T3′ vector containing *apcC* promoter by the In-Fusion cloning kit.

Microscopic examination of *C. merolae* cells

For observation of GFP fluorescence, transformed *C. merolae* cells were centrifuged at 200*g* for 10 min, and then examined using a BX-60 fluorescence microscope (Olympus, Tokyo, Japan) equipped with a narrowband filter cube (U-MNIBA; Olympus). Immunofluorescence detection was performed essentially according to Nishida et al. (2004). In the primary antibody reaction, anti-GFP or anti-HA-tag monoclonal antibodies diluted to 1/200 with immunoreaction enhancer solution (Can Get Signal Immunostain Solution B; Toyobo, Osaka, Japan) were reacted with cells for 1 h. As the secondary antibody, anti-mouse IgG monoclonal antibody labeled with Alexa fluor 488 (Invitrogen) was diluted to 1/200 with immunoreaction enhancer solution and reacted for 30 min. For immunofluorescence detection using the Tyramide Signal Amplification (TSA) kit (Invitrogen), the primary antibody (anti-GFP antibody) and secondary antibody (anti-mouse monoclonal antibody conjugated with horseradish peroxidase) were diluted to 1/200 and 1/100, respectively. The immunolabelled cells were observed under a fluorescence microscope equipped with a cube U-MNIBA for Alexa fluor 488, and a cube U-MWIG (Olympus) for the detection of chlorophyll autofluorescence. Nomarski differential interference images were also recorded. All microscopic images were captured using a digital camera (model DP-70; Olympus) and processed by Photoshop (Adobe, San Jose, CA, USA).

Results

Enzymes related to carbohydrate metabolism in the *C. merolae* genome

Enzymes related to glycolysis, oxPPP, and the TCA and Calvin–Benson cycles in *C. merolae* were identified in the KEGG pathway (http://www.genome.jp/kegg/pathway.html) and Gclust databases (http://gclust.c.u-tokyo.ac.jp/; Sato 2009) are listed in Table 1. The analysis revealed that the *C. merolae* genome encodes complete sets of enzymes for glycolysis, and the TCA and Calvin–Benson cycles. However, transaldolase (TAL, ID: 18), which is an oxPPP enzyme, was not found in the genome. Among the identified enzymes involved in carbohydrate metabolism, four enzymes, PDH-E1 alpha and beta, RBCL, and RBCS, were

Table 1 List of enzymes related to glycolysis, oxidative pentose phosphate pathway, Calvin–Benson cycle, and TCA cycle in *C. merolae* and summary of localization analysis

Annotation	EC no.	Accession no.	Protein name	TargetP	Wolf PSORT	Confirmed localization
Glycolysis/gluconeogenesis						
Glucokinase	2.7.1.2	CMO276C	GLK	None	Pt	Cyto
Phosphoglucomutase	5.4.2.2	CMJ272C	PGM-1	None	Nuc	Pt
		CMT285C	PGM-2	None	Cytosk	Cyto
Phosphoglucose isomerase	5.3.1.9	CMO124C	PGI-1	Pt	Pt	Pt
		CMT497C	PGI-2	Mt	Mt	Cyto
Phosphofructokinase, ATP-dependent	2.7.1.11	CMI162C	PFK-1	None	Cyto	Cyto
		CMM196C	PFK-2	Pt	Pt	Pt
Phosphofructokinase, PPi-dependent	2.7.1.90	CMH052C	PFP	None	Pt	Cyto
Fructose-1,6-bisphosphatase	3.1.3.11	CMD041C	FBP-1	None	ER	Cyto
		CMO245C	FBP-2	Pt	Pt	Pt
		CMP129C	FBP-3	None	Pt	Cyto
Fructose-1,6-bisphosphate aldolase	4.1.2.13	CME145C	FBA-1	None	Cyto	Cyto
		CMI049C	FBA-2	Pt	Pt	Pt
Triosephosphate isomerase	5.3.1.1	CMQ172C	TPI	Mt	Pt	Cyto, Pt
GAP dehydrogenase, NAD^+-dependent, phosphorylating	1.2.1.12	CMJ250C	GAPC-1	Mt	Cyto	Cyto
		CMM167C	GAPC-2	None	Cyto	Cyto
GAP dehydrogenase, $NADP^+$-dependent, phosphorylating	1.2.1.13	CMJ042C	GAPA	Pt	Cyto	Pt
GAP dehydrogenase, $NADP^+$-dependent, non-phosphorylating	1.2.1.9	CMT034C	GAPN	None	Pt	Cyto
Phosphoglycerate kinase	2.7.2.3	CMJ305C	PGK	Pt	Pt	Cyto, Pt
Phosphoglycerate mutase	5.4.2.1	CMK188C	PGAM	Secretory	Cyto	Cyto
Enolase	4.2.1.11	CMK131C	ENO	None	Cyto	Cyto
Pyruvate kinase	2.7.1.40	CMA030C	PK-1	Pt	Pt	Pt
		CMC021C	PK-2	Mt	Cyto	Cyto
		CMK041C	PK-3	Pt	Cyto	Pt
		CMP260C	PK-4	None	Pt	Cyto
Phospho*enol*pyruvate carboxylase	4.1.1.31	CME095C	PEPC	None	Cyto	Cyto
Phospho*enol*pyruvate carboxykinase	4.1.1.49	CMN285C	PEPCK	Mt	Mt	Cyto
Metabolism of pyruvate						
Pyruvate dehydrogenase E1	1.2.4.1	CMS327C	PDH-E1 beta	Mt	Pt	Mt
		CMT256C	PDH-E1 alpha	Mt	Mt	Mt
		CMV153C	ptPDH-E1 alpha			Pt-genome
		CMV154C	ptPDH-E1 beta			Pt-genome
Pyruvate dehydrogenase E2	2.3.1.12	CMI273C	PDH-E2-1	None	Pt	Cyto
		CMN017C	PDH-E2-2	Mt	Mt	Mt
		CMN233C	PDH-E2-3	Pt	Pt	Pt
Pyruvate dehydrogenase E3/Dihydrolipoamide dehydrogenase	1.8.1.4	CMM299C	LPD (E3)-1	Mt	Mt	Mt
		CMQ234C	LPD (E3)-2	Pt	Cyto	Pt
Malic enzyme, $NADP^+$-dependent	1.1.1.40	CMJ051C	ME	Mt	Cyto	Cyto
Oxidative and reductive pentose phosphate pathway						
Glucose-6-phosphate dehydrogenase	1.1.1.49	CMI224C	G6PDH-1	Pt	Pt	Cyto
		CMR014C	G6PDH-2	None	Pt	Pt
6-phosphogluconolactonase	3.1.1.31	CMC120C	PGL	Pt	Pt	Cyto, Pt

Table 1 continued

Annotation	EC no.	Accession no.	Protein name	TargetP	Wolf PSORT	Confirmed localization
6-phosphogluconate dehydrogenase	1.1.1.44	CML037C/ CML036C[a]	6PGDH-1	Mt	Pt	Pt
		CML059C	6PGDH-2	Mt	Pt	Pt[b]
		CMM231C	6PGDH-3	Mt	Pt	Pt[b]
		CMS195C	6PGDH-4	None	Pt	Cyto
Ribose-5-phosphate isomerase	5.3.1.6	CMO291C	RPI	Pt	Pt	Cyto, Pt
Ribulose-5-phosphate-3-epimerase	5.1.3.1	CMI084C	RPE-1	None	Plasma	Cyto
		CMO229C	RPE-2	Secretory	Extra	Cyto
		CMT633C	RPE-3	Pt	Pt	Pt
Transketolase	2.2.1.1	CMO121C	TKT-1	Pt	Pt	Pt
		CMO128C	TKT-2	Pt	Pt	Pt
Transaldolase	2.2.1.2	Not detected				
Sedoheptulose-1,7-bisphosphatase	3.1.3.37	CMI196C	SBP-1	Pt	Pt	Pt
		CMT362C	SBP-2	None	Plasma	Cyto
Phosphoribulokinase	2.7.1.19	CMF117C	PRK	Pt	Pt	Pt
Ribulose bisphosphate carboxylase	4.1.1.39	CMV013C	RBCL			Pt-genome
		CMV014C	RBCS			Pt-genome
TCA cycle						
Citrate synthase	2.3.3.1	CMA040C	CS-1	None	Cyto	Peroxi
		CMJ293C	CS-2	None	Peroxi	Peroxi
		CMM068C	CS-3	Mt	Mt	Peroxi
		CMQ191C	CS-4	Mt	Mt	Mt
Aconitase	4.2.1.3	CMT561C	ACO	Mt	Mt	Mt
Isocitrate dehydrogenase, NAD^+-dependent	1.1.1.41	CMS272C	IDH2	Mt	Mt	Mt
		CMT412C	IDH1	Mt	Pt	Mt
Isocitrate dehydrogenase, $NADP^+$-dependent	1.1.1.42	CMT216C	ICDH	Pt	Pt	Cyto
2-oxoglutarate dehydrogenase E1	1.2.4.2	CMF068C	2OGDH-E1	Mt	Pt	Mt
2-oxoglutarate dehydrogenase E2	2.3.1.61	CMJ055C	2OGDH-E2	Mt	Mt	Mt
Succinyl-CoA synthetase	6.2.1.4	CMH132C	SCS-alpha	Mt	Pt	Mt
		CMT209C	SCS-beta	Mt	Pt	Mt
Succinate dehydrogenase (Complex II) flavoprotein subunit	1.3.5.1	CMT582C	SDH1	Mt	Mt	Mt
Succinate dehydrogenase cytochrome B560 subunit		CMW001C	SDH3			Mt-genome
Succinate dehydrogenase iron-sulfur protein		CMW002C	SDH2			Mt-genome
Succinate dehydrogenase hydrophobic subunit		CMW055C	SDH4			Mt-genome
Fumarase	4.2.1.2	CMD058C	FUM	Mt	Mt	Mt
Malate dehydrogenase	1.1.1.37	CMP193C	MDH-1	Mt	Pt	Mt
		CMT611C	MDH-2	Mt	Pt	Cyto

Pt plastid, *Mt* mitochondrion, *Nuc* nucleus, *Cyto* cytosol, *Cytosk* cytoskeleton, *ER* endoplasmic reticulum, *Plasma* plasma membrane, *Extra* extracellular, *Peroxi* peroxisome

[a] Based on the re-sequencing results in the present study, CML036C and CML037C were annotated as a single enzyme (Online Resource Fig. S 1)

[b] Localization analysis was not performed because the *N*-terminal sequences of 6PGDH-2 and -3 were nearly identical with that of 6PGDH-1

encoded by the plastid genome, and three subunits of succinate dehydrogenase, SDH2, SDH3, and SDH4, were encoded by the mitochondrial genome. These enzymes were therefore speculated to be localized to the respective organelles.

In the genome database of *C. merolae* (http://merolae.biol.s.u-tokyo.ac.jp/), five gene products, CML036C, CML037C, CML059, CMM231C, and CMS195C, are annotated as 6-phosphogluconate dehydrogenases (6PGDH). CML059C (6PGDH-2), CMM231C (6PGDH-

3), and CMS195C (6PGDH-4) contain a full-length 6PGDH domain, whereas CML036C and CML037C are homologous to the *C*- and *N*-terminal regions, respectively, of 6PGDH. The open reading frames (ORFs) of CML036C and CML037C were found to overlap, with the initiation codon of CML036C predicted to be located in the latter half of CML037C. To determine whether CML036C and CML037C were different proteins, the region upstream of CML036C was sequenced, revealing that the 477th cytosine base of *CML037C* had been erroneously included in the genome sequence due to a sequencing error (Online Resource Fig. S 1a). Removal of this base resulted in a shift of the reading frame of CML037C to be in-frame with CML036C. In addition, alignment analysis of *C. merolae* 6PGDHs suggested that the start codon of CML037C/CML036C was 219 bp upstream of the first methionine of CML037C (Online Resource Fig. S 1). The amino acid sequence of CML037C/CML036C (6PGDH-1) was nearly identical with that of CML059C (99 %) and CMM231C (99 %) (Online Resource Fig. S 1b).

Subcellular localization of the identified metabolic enzymes was predicted using the computer programs TargetP (http://www.cbs.dtu.dk/services/TargetP/; Emanuelsson et al. 2007) and Wolf PSORT (http://www.genscript.com/psort/wolf_psort.html; Horton et al. 2007) (Table 1). In addition to estimation of localization to plastids and mitochondria, Wolf PSORT program can find peroxisomal targeting sequence (PTS), estimating the existence of PTS1 in two citrate synthases [CS-1 (CMA040C) and CS-2 (CMJ293C)]. We also performed alignments of the amino acid sequences to determine whether the enzymes possessed an *N*-terminal extension for organellar targeting (data not shown). Based on the results of these analyses, the subcellular localization of the central carbohydrate pathways in *C. merolae* were predicted (Fig. 1c left).

Measurement of transaldolase activity in *C. merolae* cells

A gene encoding a known transaldolase was not found in the *C. merolae* genome. Because it is possible that *C. merolae* has a transaldolase with low homology to previously characterized transaldolases, protein extracts from *C. merolae* cells were assayed for transaldolase activity. Transaldolase catalyzes the reversible conversion of GAP and sedoheptulose 7-phosphate (S7P) to erythrose 4-phosphate (E4P) and fructose 6-phosphate (F6P). Here, transaldolase activity was estimated by measuring the production of GAP from E4P and F6P. Although a positive control (yeast transaldolase) showed high activity in this assay, no activity was detected in the protein extract of *C. merolae* cells (Online Resource Fig. S 2). However, when yeast transaldolase was added to the reaction mixture containing the cell extract, transaldolase activity was detected, suggesting that the *C. merolae* cell extract did not inhibit transaldolase activity.

Localization analysis of enzymes related to carbohydrate metabolism in *C. merolae*

Cyanidioschyzon merolae is a unicellular alga with a single plastid and mitochondrion, and reproduces by binary fission (Fig. 2a). To verify the metabolic pathways predicted from the genome sequence (Fig. 1c left), the subcellular localization of 65 nuclear genome-encoded proteins expressed in *C. merolae* cells as GFP or HA-tag fusion proteins was examined. First, *C. merolae* cells transformed to express full-length enzyme-GFP fusion proteins driven by their own promoter were examined for GFP fluorescence. If the GFP fluorescence was too weak to be reliably observed, immunofluorescence was detected using an anti-GFP antibody. If necessary, the immunofluorescence signal was amplified by the tyramide signal amplification (TSA) method. If the localization of GFP-fusion could not be determined, 3× HA-tagged fusion proteins were constructed and detected by immunofluorescence using anti-HA-tag antibody. In cases when the signal still could not be observed, the putative transit peptide-GFP fusion proteins were overexpressed using the *C. merolae apcC* gene promoter (Watanabe et al. 2011).

Figure 2b shows examples of subcellular localization of the examined proteins to the cytosol (PGM-2), plastid (FBA-2), and mitochondrion (MDH-1), the dual localization of PGK enzyme to the cytosol and plastid, and the peroxisome (catalase, Imoto et al. 2013). Images of localization analysis for other carbohydrate metabolism-related proteins are shown in Online Resource Figure S 3. Among the 65 enzymes examined, 26, 17, 15, and 3 were localized to the cytosol, plastid, mitochondrion, and peroxisome, respectively. Four enzymes, PGK, 6-phosphogluconolactonase (PGL), ribose-5-phosphate isomerase (RPI), and triosephosphate isomerase (TPI), were found to be localized to both the cytosol and plastid. The localization results for each enzyme are shown as merged images next to the respective reaction in the carbohydrate metabolic pathways in *C. merolae* (Fig. 3).

Glycolysis in *C. merolae*

Subcellular localization analysis revealed that a complete set of glycolytic enzymes, from glucokinase to pyruvate kinase (ID: 1–10), exists in the cytosol of *C. merolae* (Fig. 3). Pyrophosphate (PPi)-dependent phosphofructokinase (PFP) and $NADP^+$-dependent-non-phosphorylating GAP dehydrogenase (GAPN) are cytosolic enzymes in plants. The genome of *C. merolae* encodes one *PFP* and

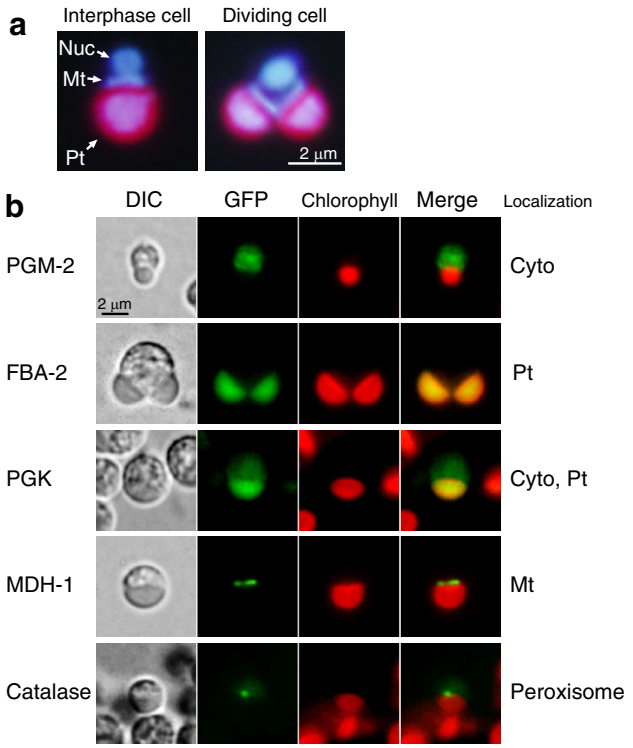

Fig. 2 Localization of GFP-fusion proteins in *C. merolae* cells. **a** Fluorescence images with 4′,6-diamidino-2-phenylindole (DAPI) staining of an interphase cell (*left*) and a dividing cell (*right*). *Nuc* nucleus, *Mt* mitochondrion, *Pt* plastid. This figure was adopted from Moriyama et al. (2014) with permission of the publisher. **b** Fluorescence microscopic images of transiently transformed *C. merolae* cells. Representative images of enzymes localized to the cytosol (PGM-2), plastid (FBA-2), both the cytosol and plastid (PGK), mitochondrion (MDH-1), and the peroxisome (catalase, Imoto et al. 2013) are shown. FBA-2, PGK, MDH-1, and catalase were observed with GFP fluorescence. PGM-2 was observed by immunofluorescence with anti-GFP antibody. Other images of GFP- and 3× HA-fusion protein analyses are shown in Online Resource Figure S 3. DIC, Normarski differential interference contrast images; Chlorophyll, chlorophyll autofluorescence; Merge, merged images of green fluorescence and chlorophyll autofluorescence; *Cyto* cytosol

one *GAPN* gene, whose protein products were localized to the cytosol, as expected. *A. thaliana* has two NAD^+-dependent GAPDHs (GAPC1 and GAPC2), which are localized to both the nucleus and cytosol (Holtgrefe et al. 2008). Nuclear-localized GAPDHs are speculated to function in stress signal transduction due to their DNA-binding ability. *C. merolae* was predicted to encode two GAP dehydrogenases (GAPC-1 and -2). GAPC-1 showed typical localization to the cytosol, whereas the GAPC-2-GFP fusion protein was observed as granules in the cytosol. For both GAPCs, nuclear localization was not observed; however, under stressful culture conditions, such as in medium containing H_2O_2 or nitric oxide (NO), GAPC-1 and -2 may be localized to the nucleus, as occurs in animals (Hara et al. 2006). Plants have alternative pathways for

Fig. 3 Central carbohydrate metabolic pathways in *C. merolae* based on subcellular localization analysis. Merged images of green fluorescence by the observation of GFP- or HA tagged-fusion proteins, chlorophyll autofluorescence (*red fluorescence*), and Normarski differential interference contrast images (*gray scale*) are overlaid on the arrow for the corresponding enzymatic reaction on the metabolic map. *Black arrows* show the glycolysis pathway in the cytosol and plastid. *Blue arrows* with a *dashed line* show oxPPP and *green lines* and *arrows* indicate the Calvin–Benson cycle. The TCA cycle is shown in mitochondrion with *black arrows*. Color-coding of enzyme names indicates the construction of fusion genes and detection methods used for determination of subcellular localization. The description of the color codes is shown in the *lower right-hand* table. *Single* and *double asterisks* indicate enzymes encoded by the plastid and mitochondrial genomes, respectively. *Triple asterisks* indicate enzymes with *N*-terminal sequences that have high homology to that of 6PGDH-1 (no localization analysis was performed for these two enzymes). Abbreviations of intermediates: *1,3BPG* 1,3-bisphoglycerate, *2OG* 2-oxoglutarate, *2PGA* 2-phosphoglycerate, *3PGA* 3-phosphoglycerate, *6PG* 6-phosphogluconate, *AcCoA* acetyl-CoA, *CIT* citrate; *DHAP* dihydroxyacetone phosphate, *E4P* erythrose 4-phosphate, *F1,6BP* fructose 1,6-bisphosphate, *F6P* fructose 6-phosphate, *FUM* fumarate, *G1P* Glucose 1-phosphate, *G6P* glucose 6-phosphate, *GAP* glyceraldehyde 3-phosphate, *GLC* glucose, *GLP* glucono 1,5-lactone 6-phosphate, *ICIT* isocitrate, *MAL* malate, *OAA* oxaloacetate, *PEP* phospho*enol*pyruvate, *PYR* pyruvate, *R5P* ribose 5-phosphate, *Ru5P*, ribulose 5-phosphate, *RuBP* ribulose 1,5-bisphosphate, *S1,7BP*, sedoheptulose 1,7-bisphosphate, *S7P* sedoheptulose 7-phosphate, *SUC* succinate, *SucCoA* succinyl-CoA, *Xu5P* xylulose 5-phosphate. Unabridged enzyme names are shown in Table 1

phospho*enol*pyruvate (PEP) metabolism in the cytosol. PEP carboxylase (PEPC) catalyzes the irreversible conversion of PEP and HCO_3^- to oxaloacetate (OAA) and orthophosphate (Pi). Conversely, OAA is converted to PEP by ATP-dependent PEP carboxykinase (PEPCK) and can be also converted to malate by malate dehydrogenase (MDH), the product of which is a substrate of malic enzyme (ME) to yield pyruvate. The enzymes related to the PEP pathway are conserved in *C. merolae* and are localized to the cytosol (Fig. 3).

Seven glycolytic enzymes, from PGI to PGK, were localized to the plastid (ID: 1–7) (Fig. 3). Furthermore, two pyruvate kinases (PKs) and pyruvate dehydrogenase E2 and E3 (PDH-E2-3 and LPD[E3]-2) were also targeted to the plastid (ID: 10 and 11), although phosphoglycerate mutase (PGAM, ID: 8) and enolase (ENO, ID: 9) were observed in the cytosol, not in the plastid. These findings are supported by the fact that two E1 subunits of PDH, alpha and beta, are encoded by the plastid genome in *C. merolae*. The *Arabidopsis* genome encodes three $NADP^+$-dependent GAPDHs (GAPA1, GAPA2, and GAPB), which function as Calvin–Benson cycle enzymes and are localized to plastids (Muñoz-Bertomeu et al. 2009). In addition to these GAPDHs, *Arabidopsis* has two NAD^+-dependent GAPDHs (GAPCp1 and 2) that are also localized to plastids (Muñoz-Bertomeu et al. 2009). The two GAPCps are mainly expressed in roots, where the enzymes play an

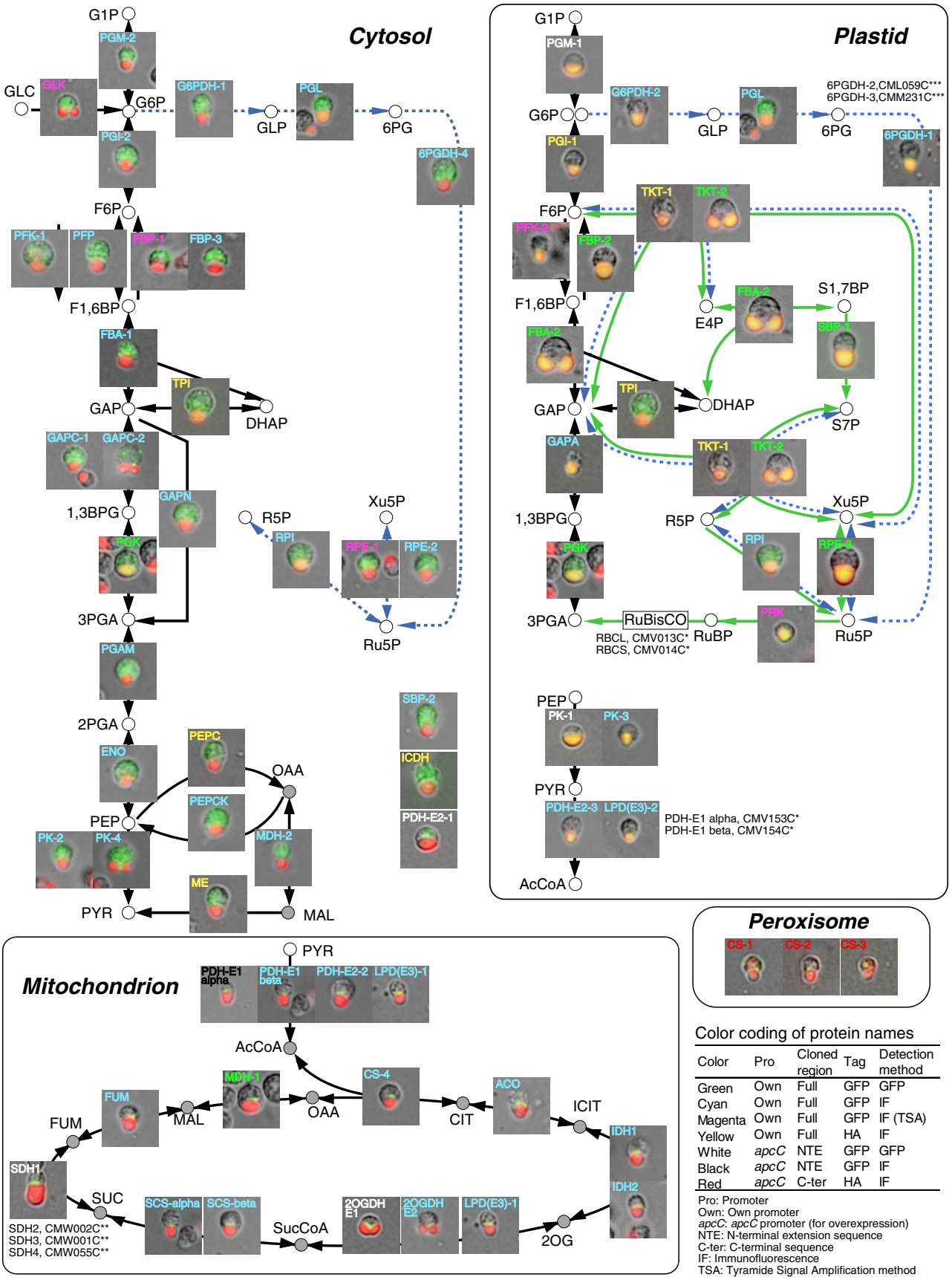

Color coding of protein names

Color	Pro	Cloned region	Tag	Detection method
Green	Own	Full	GFP	GFP
Cyan	Own	Full	GFP	IF
Magenta	Own	Full	GFP	IF (TSA)
Yellow	Own	Full	HA	IF
White	*apcC*	NTE	GFP	GFP
Black	*apcC*	NTE	GFP	IF
Red	*apcC*	C-ter	HA	IF

Pro: Promoter
Own: Own promoter
apcC: *apcC* promoter (for overexpression)
NTE: N-terminal extension sequence
C-ter: C-terminal sequence
IF: Immunofluorescence
TSA: Tyramide Signal Amplification method

important role in serine synthesis. In *C. merolae*, GAPC was localized to the cytosol, and therefore GAPA was the only plastid-localized GAPDH.

oxPPP and Calvin–Benson cycle in *C. merolae*

Oxidative pentose phosphate pathways is an alternative pathway to glycolysis for the oxidation of glucose, but this pathway mainly leads to the generation of NADPH and pentoses, rather than ATP. *C. merolae* has two glucose-6-phosphate dehydrogenases (G6PDHs, ID: 12). Alignment analyses with G6PDH orthologs and computational modeling for subcellular localization predicted the plastid localization of the two *C. merolae* G6PDHs. Additionally, *C. merolae* encodes a single 6-phosphogluconolactonase (PGL, ID: 13) and ribose-5-phosphate isomerase (RPI, ID: 15), both of which are predicted to be localized to the plastid (Table 1). Therefore, we speculated that most components of the oxPPP in *C. merolae* exist in the plastid (Table 1; Fig. 1c left). However, localization analysis revealed that one G6PDH (G6PDH-1) was localized to the cytosol, but not to the plastid. PGL and RPI were dually localized to the plastid and the cytosol (Fig. 3). This indicates that the components of oxPPP in the cytosol of *C. merolae* are the same as those found in *A. thaliana*.

In plant plastids, oxPPP largely overlaps with the Calvin–Benson cycle. In *C. merolae*, nearly all of the enzymes related to the Calvin–Benson cycle were localized to the plastid, as expected. *C. merolae* has two sedoheptulose-1,7-bisphosphatases (SBPs), which were previously annotated based on sequence similarity and phylogenetically classified (Matsuzaki et al. 2004). In the present analysis, SBP-1 was localized to the plastid, whereas SBP-2 was observed in the cytosol. Cytosolic SBP was also reported in the diatom *Phaeodactylum tricornutum*, but its function is unknown (Gruber et al. 2009).

TCA cycle in *C. merolae*

A complete set of TCA cycle enzymes, including PDH, which catalyzes the conversion of acetyl-CoA from pyruvate, were clearly localized to the mitochondrion of *C. merolae* (Fig. 3). In the present analysis, all mitochondrially localized proteins were enzymes related to the TCA cycle, and no enzymes related to glycolysis or oxPPP were found to be localized to the mitochondrion. The *C. merolae* genome encodes four citrate synthase (CS) genes; CS-4 was localized to the mitochondrion, whereas CS-1, CS-2, and CS-3 were observed in the cytosol when the constructs of *CS-GFP* fusion genes were introduced (Online Resource Fig. S 3 c, d). Since CS-1 and CS-2 are predicted to contain PTS1 at the *C*-terminus, 3× HA-tag-*CS* fusion genes (also including CS-3) expressed by the *apcC* promoter were constructed. CS-1, CS-2, and CS-3 were localized to the peroxisome (Fig. 3). Two types of isocitrate dehydrogenase, an NAD^+-dependent type (IDH) and $NADP^+$-dependent type (ICDH), are encoded by the *C. merolae* genome. In *C. merolae*, two IDHs were localized to mitochondria, and ICDH was localized to the cytosol, as is found in plants (Mhamdi et al. 2010). In plants, NAD^+-dependent MEs are present in mitochondria, where they are speculated to function in the coordination of carbon and nitrogen metabolism during the night (Tronconi et al. 2008). NAD^+-ME is widely conserved in plants and algae, although it was reported that this enzyme is not essential for the normal growth of C3 plants, such as *Arabidopsis* and tomato (Jenner et al. 2001; Tronconi et al. 2008). *C. merolae* was found to have cytosolic $NADP^+$-ME, but not NAD^+-ME.

Discussion

In the present study, we identified the enzymes related to central carbohydrate metabolism, glycolysis, oxPPP, and the Calvin–Benson and TCA cycles in the genome of *C. merolae*, and deduced their subcellular localization using targeting prediction programs and alignment analysis. These in silico analyses indicated that the *C. merolae* cytosol contains fragments of the glycolytic pathway and oxPPP (Fig. 1c), and lacked five enzymes. The *C. merolae* genome contains a single gene encoding TPI, PGK, PGL and RPI, which were predicted to be localized to the plastid. However, subcellular localization analysis revealed that these enzymes are localized to both the plastid and cytosol. Notably, all of these enzymes harbor a second methionine that is positioned near the start methionine of the bacterial and eukaryotic cytosolic enzymes used in the alignment (Online Resource Fig. S 4), suggesting that the *C. merolae* enzymes might be translated from two different methionine residues, yielding plastid- and cytosol-localized proteins, respectively. The fifth enzyme with unexpected localization is G6PDH. *C. merolae* encodes two G6PDHs harboring an *N*-terminal extension sequence; G6PDH-2 was localized to the plastid, whereas G6PDH-1 was unexpectedly localized to the cytosol. Taken together, these results demonstrate the importance of performing localization experiments to complement in silico analysis. In particular, it is difficult to predict the dual localization of a protein to the cytosol and an organelle. In the present study, most GFP- and HA-fusion genes, with the exception of six genes (Online Resource Fig. S 3e, f), were expressed by the native promoter of the target gene rather than an overexpression promoter to examine localization of enzymes translated from native start codon(s) including non-AUG start codon, an approach that appears to allow the detection of dual localization.

oxPPP in the plastid of *C. merolae*

Transaldolase is an oxPPP enzyme that catalyzes the reversible conversion of GAP and S7P to F6P and E4P. Although this enzyme is conserved in almost all organisms, the sequence identity among transaldolases is low, and the enzyme family is classified into five subfamilies (Samland et al. 2012). *A. thaliana* has two TALs, which belong to subfamilies 2 and 3, and are predicted to be localized to plastids (Kleffmann et al. 2004; Zybailov et al. 2008). Potato TAL and two tomato TALs have also been isolated and examined for tissue-specific expression and enzymatic activity (Moehs et al. 1996; Caillau and Quick 2005), but mutational analysis of TAL has not been reported. The *TAL* gene is not encoded by the *C. merolae* genome and was also not found in the EST sequence of *Porphyridium purpureum* strain CCMP 1328 (Bhattacharya et al. 2013) or the draft genome sequence of *P. purpureum* strain NIES 2140 (Tajima et al. unpublished data). However, homologs of the *TAL* gene was found in the sequenced genomes of other red algae, including *Galdieria sulphuraria* (Schönknecht et al. 2013; XP_005706833.1), *Calliarthron tuberculosum* (Chan et al. 2011; IDg12772t1), *Chondrus crispus* (Collén et al. 2013; XP_005719053.1), and *Pyropia yezoensis* (Nakamura et al. 2013; contig_22126_g5464). These facts suggest that the *TAL* gene is not uniformly distributed in red algae. To investigate if an unknown enzyme with transaldolase activity was expressed in *C. merolae*, the transaldolase activity of protein extracts from *C. merolae* cells was measured, but no activity was detected (Online Resource Fig. S 2). However, it is possible that *C. merolae* has cellular transaldolase activity, but that the enzyme(s) may require a cofactor and/or a coenzyme for activity that was not present in the reaction mixture.

Because *C. merolae* plastids lack TAL, it is speculated that S7P is produced under dark conditions by the activity of transketolase (TKT) and accumulates without further consumption. Under light conditions, S7P is produced in the Calvin–Benson cycle by SBP from sedoheptulose-1,7-bisphosphate (S1,7BP) and is consumed by TKT, indicating that the absence of TAL does not affect metabolic flow. It was previously shown that *E. coli* has an alternative pathway for S7P consumption that does not utilize TAL (Nakahigashi et al. 2009). In this pathway, S7P is converted by glycolytic ATP-dependent phosphofructokinase (PFK) into S1,7BP, which is further converted into E4P and DHAP by the glycolytic enzyme fructose-1,6-bisphosphate aldolase (FBA) (Nakahigashi et al. 2009). The authors also showed that recombinant PFKs of *E. coli* and the lactic bacterium *Lactococcus lactis*, which does not possess a *tal* gene, utilize S7P as a substrate to yield S1,7BP through the activity of a phosphotransferase. The conversion of S7P into S1,7BP by a PPi-dependent phosphofructokinase (PFK) was also reported in the parasitic amoeba *Entamoeba histolytica* (Susskind et al. 1982). Based on these reports, it is presumed that S7P is converted to S1,7BP by PFK-2 in *C. merolae* plastids, which intrinsically lack the *TAL* gene, and S1,7BP is then converted to E4P and DHAP by FBA-2 under dark conditions, as is observed in transaldolase mutants in *E. coli* (Nakahigashi et al. 2009, Fig. 4).

Carbohydrate metabolic pathways in photosynthetic eukaryotes

The present findings for *C. merolae* demonstrate that the cytosol contains the entire glycolytic pathway (ID: 1–10) and the first part of oxPPP (ID: 1–16), whereas the plastid contains an incomplete glycolytic pathway (ID: 1–7 and 10–11) and an entire oxPPP (ID: 12–17) that differs from other organisms and is presumably complemented by PFK (ID: 2) and FBA (ID: 4). In addition, *C. merolae* has sets of enzymes of the Calvin–Benson and TCA cycles in the plastid and mitochondrion, respectively, as expected. The subcellular distribution of these pathways in *C. merolae* is consistent with that in the photosynthetic tissue of *A. thaliana* (Fig. 1). Compared with *C. merolae* and *A. thaliana*, *C. reinhardtii* has less duplication of glycolysis- and oxPPP-related enzymes between the plastid and cytosol. However, as the compartmentation analyses of carbohydrate metabolic enzymes in *C. reinhardtii* were based on proteome analysis and measurement of enzymatic activity using isolated organelles and cytosol, it is possible that less abundant enzymes were not be detected. Thus, *C. reinhardtii* may have similar pathways to those in *C. merolae* and *A. thaliana*, although further studies are needed to confirm this speculation. It was reported that the subcellular distribution of metabolic pathways in diatoms are unique compared with photosynthetic eukaryotes harboring primary plastids (Kroth et al. 2008; Gruber et al. 2009; Fig. 1). Glycolysis and oxPPP are predicted to be incompletely localized to both the cytosol and plastids. In addition to the cytosol and plastid, enzymes of the lower half of the glycolysis pathway, GAPDH, PGK, PGAM, ENO, and PK (ID: 6–10), also exist in the mitochondria of diatoms (Fig. 1) (Liaud et al. 2000). Mitochondria-associated glycolytic enzymes were also reported in *A. thaliana*. These enzymes are located on the mitochondrial outer membrane, but are not found in the matrix; this spatial configuration is considered to allow the direct supply of pyruvate as a respiratory substrate (Giegé et al. 2003). In the present localization analysis in *C. merolae*, an association with the mitochondrion was not observed for any cytosol-localized glycolytic enzymes. The failure

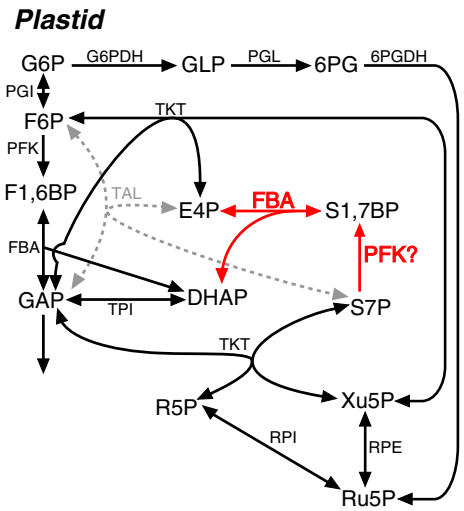

Fig. 4 A proposed model of the oxidative pentose phosphate pathway in the plastid of *C. merolae*. Details of this model are explained in the "Discussion" section. *Black arrows* show the conserved reactions of oxPPP in *C. merolae*. *Red arrows* show the putative reaction steps that are catalyzed by glycolytic PFK and FBA in *C. merolae*, which inherently lacks the *TAL* gene. *Gray arrows* with a *dashed line* indicate reactions catalyzed by TAL, which is conserved in most organisms

to detect such an association may have been caused by artifacts resulting from the use of fusion proteins or the immunodetection and cell fixation procedure. It is also possible that the extremely small cell size and volume of *C. merolae* would obviate the need for glycolytic enzymes to bind the mitochondrion for the efficient metabolic flow of glycolysis through the TCA cycle.

Plants have a glyoxylate cycle that is mainly localized to the glyoxysome (peroxisome), and consists of five enzymes: glyoxysomal malate synthase, malate dehydrogenase, citrate synthase, isocitrate lyase, and cytosolic aconitase (Graham 2008). In this cycle, acetyl CoA produced by the β-oxidation of fatty acids is finally converted into succinate. Although *C. reinhardtii* also utilizes the glyoxylate cycle (Plancke et al. 2014), we did not detect genes encoding malate synthase or isocitrate lyase in the *C. merolae* genome. Additionally, the peroxisomal localization of malate dehydrogenase or the cytosolic localization of aconitase were not observed. These results suggest that *C. merolae* does not possess a glyoxylate cycle. In *Arabidopsis*, a route for moving peroxisomal acetyl-CoA to the mitochondria was reported (Pracharoenwattana et al. 2005). In the route, oxaloacetate is imported into peroxisomes from mitochondria, which is converted to citrate by peroxisomal citrate synthase using acetyl-CoA produced from β-oxidation, then citrate is exported to the mitochondria. In *C. merolae*, three peroxisomal citrate synthases, CS-1, CS-2, and CS-3 might function in the route as in *Arabidopsis*.

Author contribution TM and NS conceived this study. All authors designed and evaluated the experiments. TM performed the experiments. TM and NS wrote the manuscript.

Acknowledgments The authors thank Dr. H. Yoshikawa and Dr. S. Watanabe of the Tokyo University of Agriculture for providing pCG1 plasmid, and also thank Dr. M. Ohnuma and T. Kuroiwa of Rikkyo University for providing plasmid pBSHAb-T3′. This work was supported in part by Core Research for Evolutional Science and Technology (CREST) from the Japan Science and Technology Agency (JST), and Grants-in-Aid for Young Scientists (B) from JSPS (No. 25870155).

References

Andriotis VM, Kruger NJ, Pike MJ, Smith AM (2010) Plastidial glycolysis in developing *Arabidopsis* embryos. New Phytol 185:649–662

Barbier G, Oesterhelt C, Larson MD, Halgren RG, Wilkerson C, Garavito RM, Benning C, Weber AP (2005) Comparative genomics of two closely related unicellular thermo-acidophilic red algae, *Galdieria sulphuraria* and *Cyanidioschyzon merolae*, reveals the molecular basis of the metabolic flexibility of *Galdieria sulphuraria* and significant differences in carbohydrate metabolism of both algae. Plant Physiol 137:460–474

Bhattacharya D, Price DC, Chan CX, Qiu H, Rose N, Ball S, Weber AP, Arias MC, Henrissat B, Coutinho PM, Krishnan A, Zäuner S, Morath S, Hilliou F, Egizi A, Perrineau MM, Yoon HS (2013) Genome of the red alga *Porphyridium purpureum*. Nat Commun 4:1941

Caillau M, Quick WP (2005) New insights into plant transaldolase. Plant J 43:1–16

Chan CX, Yang EC, Banerjee T, Yoon HS, Martone PT, Estevez JM, Bhattacharya D (2011) Red and green algal monophyly and extensive gene sharing found in a rich repertoire of red algal genes. Curr Biol 21:328–333

Chiu W, Niwa Y, Zeng W, Hirano T, Kobayashi H, Sheen J (1996) Engineered GFP as a vital reporter in plants. Curr Biol 6:325–330

Collén J, Porcel B, Carré W, Ball SG, Chaparro C, Tonon T, Barbeyron T, Michel G, Noel B, Valentin K, Elias M, Artiguenave F, Arun A, Aury JM, Barbosa-Neto JF, Bothwell JH, Bouget FY, Brillet L, Cabello-Hurtado F, Capella-Gutiérrez S, Charrier B, Cladière L, Cock JM, Coelho SM, Colleoni C, Czjzek M, Da Silva C, Delage L, Denoeud F, Deschamps P, Dittami SM, Gabaldón T, Gachon CM, Groisillier A, Hervé C, Jabbari K, Katinka M, Kloareg B, Kowalczyk N, Labadie K, Leblanc C, Lopez PJ, McLachlan DH, Meslet-Cladiere L, Moustafa A, Nehr Z, Nyvall Collén P, Panaud O, Partensky F, Poulain J, Rensing SA, Rousvoal S, Samson G, Symeonidi A, Weissenbach J, Zambounis A, Wincker P, Boyen C (2013) Genome structure and metabolic features in the red seaweed *Chondrus crispus* shed light on evolution of the Archaeplastida. Proc Natl Acad Sci 110:5247–5252

Dennis DT, Miernyk JA (1982) Compartmentation of nonphotosynthetic carbohydrate metabolism. Annu Rev Plant Physiol 33:27–50

Emanuelsson O, Brunak S, von Heijne G, Nielsen H (2007) Locating proteins in the cell using TargetP, SignalP and related tools. Nat Protoc 2:953–971

Giegé P, Heazlewood JL, Roessner-Tunali U, Millar AH, Fernie AR, Leaver CJ, Sweetlove LJ (2003) Enzymes of glycolysis are

functionally associated with the mitochondrion in *Arabidopsis* cells. Plant Cell 15:2140–2151

Graham IA (2008) Seed storage oil mobilization. Annu Rev Plant Biol 59:115–142

Gruber A, Weber T, Bártulos CR, Vugrinec S, Kroth PG (2009) Intracellular distribution of the reductive and oxidative pentose phosphate pathways in two diatoms. J Basic Microbiol 49:58–72

Hara MR, Cascio MB, Sawa A (2006) GAPDH as a sensor of NO stress. Biochim Biophys Acta 1762:502–509

Holtgrefe S, Gohlke J, Starmann J, Druce S, Klocke S, Altmann B, Wojtera J, Lindermayr C, Scheibe R (2008) Regulation of plant cytosolic glyceraldehyde 3-phosphate dehydrogenase isoforms by thiol modifications. Physiol Plant 133:211–228

Horton P, Park K, Obayashi T, Fujita N, Harada H, Adams-Collier CJ, Nakai K (2007) WoLF PSORT: protein localization predictor. Nucleic Acids Res 35:W585–W587

Imoto Y, Kuroiwa H, Yoshida Y, Ohnuma M, Fujiwara T, Yoshida M, Nishida K, Yagisawa F, Hirooka S, Miyagishima SY, Misumi O, Kawano S, Kuroiwa T (2013) Single-membrane-bounded peroxisome division revealed by isolation of dynamin-based machinery. Proc Natl Acad Sci 110:9583–9588

Jenner HL, Winning BM, Millar AH, Tomlinson KL, Leaver CJ, Hill SA (2001) NAD malic enzyme and the control of carbohydrate metabolism in potato tubers. Plant Physiol 126:1139–1149

Johnson X, Alric J (2013) Central carbon metabolism and electron transport in *Chlamydomonas reinhardtii*: metabolic constraints for carbon partitioning between oil and starch. Eukaryot Cell 12:776–793

Kleffmann T, Russenberger D, von Zychlinski A, Christopher W, Sjölander K, Gruissem W, Baginsky S (2004) The *Arabidopsis thaliana* chloroplast proteome reveals pathway abundance and novel protein functions. Curr Biol 14:354–362

Kroth PG, Chiovitti A, Gruber A, Martin-Jezequel V, Mock T, Parker MS, Stanley MS, Kaplan A, Caron L, Weber T, Maheswari U, Armbrust EV, Bowler C (2008) A model for carbohydrate metabolism in the diatom *Phaeodactylum tricornutum* deduced from comparative whole genome analysis. PLoS One 3:e1426

Liaud MF, Lichtlé C, Apt K, Martin W, Cerff R (2000) Compartment-specific isoforms of TPI and GAPDH are imported into diatom mitochondria as a fusion protein: evidence in favor of a mitochondrial origin of the eukaryotic glycolytic pathway. Mol Biol Evol 17:213–223

Matsuzaki M, Misumi O, Shin-I T, Maruyama S, Takahara M, Miyagishima SY, Mori T, Nishida K, Yagisawa F, Nishida K, Yoshida Y, Nishimura Y, Nakao S, Kobayashi T, Momoyama Y, Higashiyama T, Minoda A, Sano M, Nomoto H, Oishi K, Hayashi H, Ohta F, Nishizaka S, Haga S, Miura S, Morishita T, Kabeya Y, Terasawa K, Suzuki Y, Ishii Y, Asakawa S, Takano H, Ohta N, Kuroiwa H, Tanaka K, Shimizu N, Sugano S, Sato N, Nozaki H, Ogasawara N, Kohara Y, Kuroiwa T (2004) Genome sequence of the ultrasmall unicellular red alga *Cyanidioschyzon merolae* 10D. Nature 428:653–657

Meile L, Rohr LM, Geissmann TA, Herensperger M, Teuber M (2001) Characterization of the D-xylulose 5-phosphate/D-fructose 6-phosphate phosphoketolase gene (xfp) from *Bifidobacterium lactis*. J Bacteriol 183:2929–2936

Mhamdi A, Mauve C, Gouia H, Saindrenan P, Hodges M, Noctor G (2010) Cytosolic NADP-dependent isocitrate dehydrogenase contributes to redox homeostasis and the regulation of pathogen responses in *Arabidopsis* leaves. Plant Cell Environ 33:1112–1123

Minoda A, Sakagami R, Yagisawa F, Kuroiwa T, Tanaka K (2004) Improvement of culture conditions and evidence for nuclear transformation by homologous recombination in a red alga, *Cyanidioschyzon merolae* 10D. Plant Cell Physiol 45:667–671

Moehs CP, Allen PV, Friedman M, Belknap WR (1996) Cloning and expression of transaldolase from potato. Plant Mol Biol 32:447–452

Moriyama T, Terasawa K, Fujiwara M, Sato N (2008) Purification and characterization of organellar DNA polymerases in the red alga *Cyanidioschyzon merolae*. FEBS J 275:2899–2918

Moriyama T, Tajima N, Sekine K, Sato N (2014) Localization and phylogenetic analysis of enzymes related to organellar genome replication in the unicellular rhodophyte *Cyanidioschyzon merolae*. Genome Biol Evol 6:228–237

Muñoz-Bertomeu J, Cascales-Miñana B, Mulet JM, Baroja-Fernández E, Pozueta-Romero J, Kuhn JM, Segura J, Ros R (2009) Plastidial glyceraldehyde-3-phosphate dehydrogenase deficiency leads to altered root development and affects the sugar and amino acid balance in *Arabidopsis*. Plant Physiol 151:541–558

Nakahigashi K, Toya Y, Ishii N, Soga T, Hasegawa M, Watanabe H, Takai Y, Honma M, Mori H, Tomita M (2009) Systematic phenome analysis of *Escherichia coli* multiple-knockout mutants reveals hidden reactions in central carbon metabolism. Mol Syst Biol 5:306

Nakamura Y, Sasaki N, Kobayashi M, Ojima N, Yasuike M, Shigenobu Y, Satomi M, Fukuma Y, Shiwaku K, Tsujimoto A, Kobayashi T, Nakayama I, Ito F, Nakajima K, Sano M, Wada T, Kuhara S, Inouye K, Gojobori T, Ikeo K (2013) The first symbiont-free genome sequence of marine red alga, Susabi-nori (*Pyropia yezoensis*). PLoS One 8:e57122

Nishida K, Misumi O, Yagisawa F, Kuroiwa H, Nagata T, Kuroiwa T (2004) Triple immunofluorescent labeling of FtsZ, dynamin, and EF-Tu reveals a loose association between the inner and outer membrane mitochondrial division machinery in the red alga *Cyanidioschyzon merolae*. J Histochem Cytochem 52:843–849

Nozaki H, Takano H, Misumi O, Terasawa K, Matsuzaki M, Maruyama S, Nishida K, Yagisawa F, Yoshida Y, Fujiwara T, Takio S, Tamura K, Chung SJ, Nakamura S, Kuroiwa H, Tanaka K, Sato N, Kuroiwa T (2007) A 100 %-complete sequence reveals unusually simple genomic features in the hot-spring red alga *Cyanidioschyzon merolae*. BMC Biol 5:28

Ohnuma M, Yokoyama T, Inouye T, Sekine Y, Tanaka K (2008) Polyethylene glycol (PEG)-mediated transient gene expression in a red alga, *Cyanidioschyzon merolae* 10D. Plant Cell Physiol 49:117–120

Ohta N, Sato N, Kuroiwa T (1998) Structure and organization of the mitochondrial genome of the unicellular red alga *Cyanidioschyzon merolae* deduced from the complete nucleotide sequence. Nucleic Acids Res 26:5190–5198

Ohta N, Matsuzaki M, Misumi O, Miyagishima S, Nozaki H, Tanaka K, Shin-I T, Kohara Y, Kuroiwa T (2003) Complete sequence and analysis of the plastid genome of the unicellular red alga *Cyanidioschyzon merolae*. DNA Res 10:67–77

Plancke C, Vigeolas H, Höhner R, Roberty S, Emonds-Alt B, Larosa V, Willamme R, Duby F, Onga Dhali D, Thonart P, Hiligsmann S, Franck F, Eppe G, Cardol P, Hippler M, Remacle C (2014) Lack of isocitrate lyase in *Chlamydomonas* leads to changes in carbon metabolism and in the response to oxidative stress under mixotrophic growth. Plant J 77:404–417

Pracharoenwattana I, Cornah JE, Smith SM (2005) Arabidopsis peroxisomal citrate synthase is required for fatty acid respiration and seed germination. Plant Cell 17:2037–2048

Racker E (1962) Fructose-6-phosphate phosphoketolase from *Acetobacter xylinum*. Methods Enzymol 5:276–280

Samland AK, Baier S, Schürmann M, Inoue T, Huf S, Schneider G, Sprenger GA, Sandalova T (2012) Conservation of structure and mechanism within the transaldolase enzyme family. FEBS J 279:766–778

Sato N (2009) Gclust: trans-kingdom classification of proteins using automatic individual threshold setting. Bioinformatics 25:599–605

Sato N, Moriyama T (2007) Genomic and biochemical analysis of lipid biosynthesis in the unicellular rhodophyte *Cyanidioschyzon*

merolae: lack of a plastidic desaturation pathway results in the coupled pathway of galactolipid synthesis. Eukaryot Cell 6:1006–1017

Schönknecht G, Chen W, Ternes CM, Barbier GG, Shrestha RP, Stanke M, Bräutigam A, Baker BJ, Banfield JF, Garavito RM, Carr K, Wilkerson C, Rensing SA, Gagneul D, Dickenson NE, Oesterhelt C, Lercher MJ, Weber AP (2013) Gene transfer from bacteria and archaea facilitated evolution of an extremophilic eukaryote. Science 339:1207–1210

Soderberg T, Alver RC (2004) Transaldolase of *Methanocaldococcus jannaschii*. Archaea 1:255–262

Susskind BM, Warren LG, Reeves RE (1982) A pathway for the interconversion of hexose and pentose in the parasitic amoeba *Entamoeba histolytica*. Biochem J 204:191–196

Toda K, Takano H, Miyagishima S, Kuroiwa H, Kuroiwa T (1998) Characterization of a chloroplast isoform of serine acetyltransferase from the thermo-acidiphilic red alga *Cyanidioschyzon merolae*. Biochim Biophys Acta 1403:72–84

Tronconi MA, Fahnenstich H, Weehler MC, Andreo CS, Flügge U, Drincovich MF, Maurino VG (2008) Arabidopsis NAD-malic enzyme functions as a homodimer and heterodimer and has a major impact on nocturnal metabolism. Plant Physiol 146:1540–1552

Tyra HM, Linka M, Weber APM, Bhattacharya D (2007) Host origin of plastid solute transporters in the first photosynthetic eukaryotes. Genome Biol 8:R212

Watanabe S, Ohnuma M, Sato J, Yoshikawa H, Tanaka K (2011) Utility of a GFP reporter system in the red alga *Cyanidioschyzon merolae*. J Gen Appl Microbiol 57:69–72

Zybailov B, Rutschow H, Friso G, Rudella A, Emanuelsson O, Sun Q, van Wijk KJ (2008) Sorting signals, N-terminal modifications and abundance of the chloroplast proteome. PLoS One 3:e1994